

Hydrodynamic interactions in active colloidal crystal microrheology

R. Weeber¹ and J. Harting^{2,1}

¹*Institute for Computational Physics, University of Stuttgart,
Pfaffenwaldring 27, D-70569 Stuttgart, Germany*

²*Department of Applied Physics, Eindhoven University of Technology,
P. O. Box 513, 5600 MB Eindhoven, The Netherlands*

(Dated: June 24, 2018)

In dense colloids it is commonly assumed that hydrodynamic interactions do not play a role. However, a found theoretical quantification is often missing. We present computer simulations that are motivated by experiments where a large colloidal particle is dragged through a colloidal crystal. To qualify the influence of long-ranged hydrodynamics, we model the setup by conventional Langevin dynamics simulations and by an improved scheme with limited hydrodynamic interactions. This scheme significantly improves our results and allows to show that hydrodynamics strongly impacts on the development of defects, the crystal regeneration as well as on the jamming behavior.

PACS numbers: 47.55.Kf, 77.84.Nh, 47.11.-j

I. INTRODUCTION

Colloidal crystals are commonly studied complex fluids which allow to investigate the interplay between the local micromechanics and the macroscopic mechanical properties of the crystal. Also, they can be used as a model system for nanoscopic systems since colloids are easier to observe and manipulate than atoms due to their larger size and slower dynamics [1]. Among others, melting [2–4], defect dynamics [5, 6], phase behavior [7], and glass formation [8] have been studied with colloidal crystals. They can be manipulated on the single particle level by optical tweezers: due to electric gradient forces, particles are trapped and moved along in the focus of a laser beam [9]. For moderate displacements from the trap center the trapping potential can be approximated to be parabolic resulting in a force that is proportional to the displacement. We follow recent experiments and study a system where a large particle is dragged through a two-dimensional triangular colloidal crystal of smaller ones. All particles are suspended in water and slightly charged. The dynamical properties of the crystal, like stiffness and defect formation, can be measured directly using optical methods [4]. For numerical simulations of colloidal crystals it is commonly assumed that due to electrostatic repulsion of the particles, their dense packing and the generally moderate deformation of the crystal the system can be assumed as overdamped and long-range hydrodynamic interactions are ignored in order to reduce the computational effort [3, 10]. However, in case of optical tweezer experiments the situation is less clear. The movement of the large probe particle can deform and even locally melt the crystal. Furthermore, so as to not influence surrounding colloidal particles by the trapping laser, the driven particle has to be significantly larger than the surrounding ones. This implies that it creates significant drag on the fluid. We show that it strongly influences the healing of defects and restructuring of the crystal. Similar systems have been studied numerically earlier [3]. However, instead of pushing the probe with a

constant force, we model the moving parabolic potential of the optical tweezer and use size ratios as in experiments [4]. To demonstrate the effect of long-range hydrodynamics, the system is modeled in 3D using conventional Langevin dynamics (LD) and an improved scheme that includes limited hydrodynamics between the probe and the surrounding crystal [11–13]. The reason for this choice is two-fold: due to its computational efficiency conventional LD is the most commonly used method to simulate overdamped colloids. On the other hand, the improved scheme utilizes a correction of the velocity field as induced by the large particle. By switching between the schemes we can investigate in a simple manner the impact of the flow induced by the probe on the crystal itself.

II. SIMULATION TECHNIQUE

When a probe is dragged through a colloidal crystal, the dynamics is influenced by several factors: strong forces due to the tweezer and the electrostatic potentials between the particles exist. These forces dominate the dynamics in front of the probe. Furthermore, especially the particles behind it feel a hydrodynamics-mediated drag force in the direction of motion. This drag also exists in front of the probe, but there the system is more jammed. Behind the probe, diffusion and electrostatic repulsion among particles control the “healing” of the crystal. Our simulations utilize a modified LD method, which gives more accurate results for the drag force on the probe and to some extent models the drag exerted behind the driven particle [11]. To demonstrate the importance of long-ranged hydrodynamic effects in colloidal crystals, we compare our results to conventional LD. For overdamped systems computing time can be saved by not explicitly calculating the flow field. Instead, only the most relevant effects of the fluid on suspended particles are simulated by additional forces in a molecular dynamics (MD) algorithm: the Stokes friction and thermal fluctuation

tuations. The motion of the i 'th particle is described by the Langevin equation

$$m\ddot{\mathbf{x}}_i = \gamma\dot{\mathbf{x}}_i + \mathbf{F}_i^{\text{rnd}} + \mathbf{F}_i^0, \quad (1)$$

where γ is the friction coefficient, $\mathbf{F}_i^{\text{rnd}}$ is a random force describing Brownian motion, and \mathbf{F}_i^0 represents forces between particles (e.g. a Coulomb force) and external forces (e.g. gravity). In case of fully overdamped dynamics the inertia term can be dropped reducing the method to simplified Brownian Dynamics. However, due to the movement of the probe particle inside the optical trap inertia should not be ignored. According to the fluctuation-dissipation-theorem, the amplitude of the random force is connected with the friction coefficient of the Stokes force. It is assumed that $\mathbf{F}_i^{\text{rnd}}$ is Gaussian-distributed with zero mean and uncorrelated in time. This is a strong approximation: if one particle starts moving, it drags some of the surrounding fluid with it. This in turn drags along secondary particles in its vicinity. The mean square deviation of $\mathbf{F}_i^{\text{rnd}}$ is given by

$$\langle |\mathbf{F}_i^{\text{rnd}}|^2 \rangle = 12\pi\eta R k_B T. \quad (2)$$

LD is popular to simulate suspensions due to its simplicity and low amount of computation required. However, it completely lacks the hydrodynamic interactions between particles. In the system we consider, these interactions are, however, important: the large particle has a volume of about 125 times that of the small ones and also moves at a substantially higher velocity. Thus, it strongly influences the flow around it. Furthermore, the surrounding particles are dragged due to the motion of the probe and the flow advects crystal particles to the sides at the front of the dragged particle and back into the empty region behind it. The smaller and slower particles do not have as large impact on the flow. Therefore, it is possible to improve the LD scheme by including the flow field created by the large particle [11]: the probe still feels the Stokes friction imposed by a resting fluid with viscosity η . Small particles with velocity \mathbf{v} and radius R_{small} , however, feel a force $\mathbf{F} = 6\pi\eta R_{\text{small}}(\mathbf{v} - \mathbf{v}_f)$ due to a moving fluid as caused by the motion of the probe. Here,

$$\mathbf{v}_f(\mathbf{r}) = \frac{3R}{4r} \left[\left(1 + \frac{R^2}{3r^2} \right) \mathbf{u} + \left(1 - \frac{R^2}{r^2} \right) \hat{\mathbf{r}} (\hat{\mathbf{r}} \cdot \mathbf{u}) \right] \quad (3)$$

is the fluid velocity at the position of the small particle [14], where $\hat{\mathbf{r}}$ is the unit vector in the direction from the large to the small particle, r is their distance, and R and \mathbf{u} are the large particle's radius and velocity. As shown in this letter, this scheme significantly improves the results for suspensions, through which a colloidal particle is dragged by an optical tweezer. The streamlines on the upwind side of the probe bend around it. Thereby, they also move obstacles out of the way of the probe lowering the drag exerted on it. Also, the flow field created by the large particle drags along some of the surrounding crystal causing the movement of an effectively much

larger object. In particular behind the probe the drag is increased, since there the crystal is less jammed [12, 13]. The particles forming the crystal have a radius of $1.6\mu\text{m}$ and are kept on the bottom of the container by gravity. The surface area of the bottom of the container that has to be covered to form a stable crystal depends on the interaction potential. We consider weakly charged particles and area densities of $\sim 74\%$ resulting in a lattice spacing of $a = 3.5\mu\text{m}$. The crystal is generated by explicitly calculating the particle positions, where the stacking distance between horizontal rows is $a \sin 60^\circ = \frac{\sqrt{3}a}{2} \approx 0.866a$ and the offset in consecutive rows is $a \cos 60^\circ = \frac{a}{2}$. A screened Coulomb potential

$$V = \frac{1}{r} \exp(-\kappa(r - R_1 - R_2)), \quad (4)$$

is used to model the interactions, where κ is the inverse screening length and R_1 and R_2 are the particle radii. The potential at the surface of the colloids is 10mV and the screening length is varied between 20 and 50nm . Identical κ are chosen for the interactions between small particles and between a small and the large particle, because screening is controlled by the ion concentration in the solvent rather than by a property of the colloidal particles. The dragged particle has a radius $R = 7.75\mu\text{m}$ and the potential of the optical tweezer

$$V_{\text{trap}} = C \cdot (\mathbf{x} - \mathbf{x}_t(t))^2, \quad (5)$$

is assumed to be harmonic, where \mathbf{x} and \mathbf{x}_t are the positions of the particle, and trap center and t is time. The force constant is chosen as $C = 3.2 \cdot 10^{-7} \text{Jm}^{-2}$, which is a reasonable value for experiments: a particle with a distance of $1\mu\text{m}$ from the trap center feels a potential of $\approx 40k_B T$. The tweezer moves through the crystal with a constant velocity between $0.5\mu\text{m/s}$ and $8\mu\text{m/s}$. A long system is required since it takes up to 240s to reach the steady state – especially for simulations at low velocities including hydrodynamic corrections. I.e., for a velocity of $4\mu\text{m/s}$, the probe passes approx. $1000\mu\text{m}$, before the trapping force equals the friction on the probe. If the system is too narrow in the direction perpendicular to the drag, it gets jammed and the steady state is not reached before the probe arrives at the end of the channel. Furthermore, long-ranged electrostatic and hydrodynamic interactions can cause finite size effects. Due to strong fluctuations of the measured probe position, averaging over 60 to 100s is needed for drag force measurements rendering our simulations computationally demanding. We use a crystal of approx. 570×165 particles resulting in a system size of $2000\mu\text{m} \times 500\mu\text{m}$. The system height and timestep are $30\mu\text{m}$ and $\delta t = 98.4\mu\text{s}$. To allow for such a large time step – and therefore reducing computation time – we rescale some physical units: the suspension is simulated at a lower temperature and viscosity. To preserve the Péclet number, i.e., the relative importance of dynamics due to potentials and diffusion, all forces are scaled down by the same factor (here $1/11933$) as described in [15].

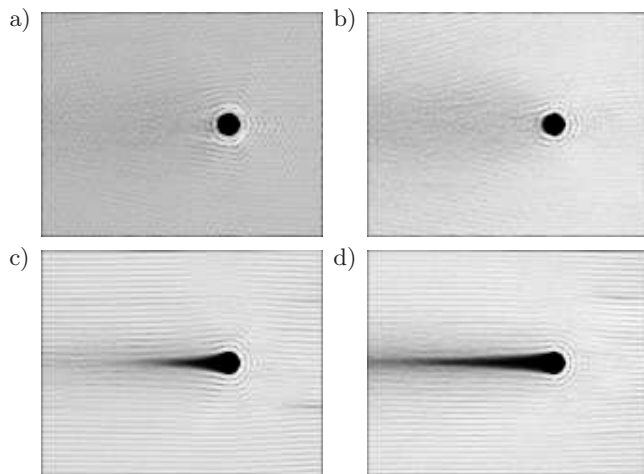


FIG. 1. Density map for $\mathbf{u} = 8\mu\text{m/s}$ and $1/\kappa = 50\text{nm}$ (left) and 20nm (right) with (upper row) and without (bottom row) hydrodynamic correction. The crystal melts in front of the probe and small particles rearrange into a circular structure. When neglecting the flow field of the probe, the lack of drag and the advection of the small particles around it cause a large depletion zone to form. With correction, this zone is substantially reduced. Healing is more efficient for larger $1/\kappa$ since particles are pushed into the empty region by electrostatic repulsion.

III. RESULTS

The volume of the probe particle is by a factor of 125 larger than that of the small ones. When it moves, it creates a significant flow around it inducing two consequences: crystal particles at the front are advected to the sides and around the probe. They then fill the depletion region and thereby weaken it. The drag force felt by the probe is reduced since the obstacles are moved to the sides without getting in contact with the probe. Furthermore, the crystal particles around the probe are dragged along with its motion leading to an effectively much larger object that is dragged through the crystal. Thus, more reorganisation has to take place leading to an increased drag. The influence of this flow field can be investigated quantitatively by comparing simulations using LD with the flow field correction as described above and conventional LD which does not include any hydrodynamics. Other hydrodynamic effects – like the influence of the surface on which the crystal lies – are not taken into account here. We first turn to the surrounding of the probe and then elaborate on the quantitative effect of the flow field on the drag force exerted on the probe.

In Fig. 1, we compare density maps for the case with and without the probe’s flow field considered. To obtain such a map, about 1000 snapshots of the crystal are taken while the probe is driven through it and moved such that the driven particle coincides in all of them. We divide the system into 150×120 bins and calculate the probability for each bin to be occupied. It can be seen that for conventional LD, a large depletion zone forms behind the

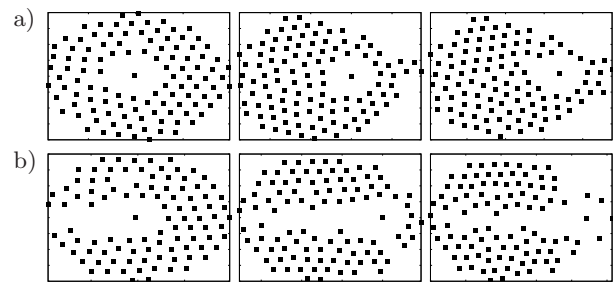


FIG. 2. Traced particle positions around the probe with (a) and without (b) the flow field of the probe taken into account. The probe moves at $5\mu\text{m/s}$. In the first time step, particles that are within a distance of $20\mu\text{m}$ of the probe’s center are marked (left). These are observed after 3s (middle) and 5s (right). If the probe’s flow field is considered, the probe is not moving individually through the crystal, but is accompanied by an entire cloud of particles. This effect is only weakly present in conventional LD simulations.

probe due to the lack of slip stream, i.e. particles do not diffuse into the depletion region. We find that this region is the more pronounced, the higher the velocity gets, because then, the probe clears more space in a given time, whereas the reconstruction process behind the probe is not directly influenced by the velocity. It is, however, controlled by three factors: diffusion, electrostatic repulsion between the crystal particles and the drag created by the driven particle. Only the latter is directly affected by \mathbf{u} . In the case with the flow field modeled, however, this depletion zone is substantially reduced. The circular structure created by the melting of the crystal close to the probe’s surface is visible in both maps. At long-ranged potentials and high velocities, layers of circularly arranged particles can be seen. With hydrodynamic correction, however, the circular structure extends further back because the flow advects crystal particles around the probe and into the depletion zone behind it.

In Fig. 2, we consider individual particles close to the probe’s surface while it moves with a velocity of $5\mu\text{m/s}$. Thereby, we study how the dynamics of the crystal particles changes due to the hydrodynamic correction. In the first time step, all particles that lie within $20\mu\text{m}$ of the probe’s center are tagged. We then follow these particles in time. In Fig. 2, the particles are shown after 3s and 5s for both, a simulation with and without hydrodynamic correction. It can be seen that when the flow field evolving around the probe is considered, the probe does not move through the crystal individually. Rather, it is accompanied by an entire cloud of smaller particles. In a conventional LD simulation, on the other hand, the surrounding particles drop behind the moving probe.

The interplay between a lower drag force due to the advection of the surrounding crystal particles and an increase due to part of the crystal moving along is studied by comparing the forces at different radii of the small particles. In Fig. 3, the displacement of the probe is shown versus radii of the small particles between $1.45\mu\text{m}$ and

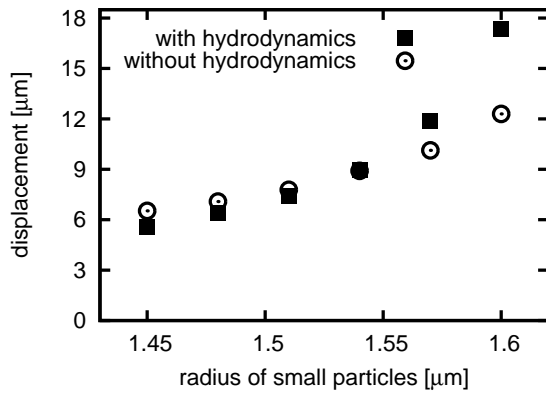


FIG. 3. Displacement of the probe versus the small particles' radius with and without hydrodynamics considered. All simulations were performed at a drag velocity of $4\mu\text{m/s}$ and $1/\kappa = 40\text{nm}$. It can be seen that for smaller radii, the hydrodynamic interactions lower the drag force acting on the probe due to the advection of crystal particles around it. For larger radii, the system becomes jammed and hydrodynamics results in an additional friction due to the increased level of rearrangement in the surrounding crystal.

$1.6\mu\text{m}$, both, with and without hydrodynamic correction. At a radius of about $1.54\mu\text{m}$, the same drag is obtained for both cases. Below this point, the force is lower if hydrodynamic corrections are applied because of the advection of crystal particles around the probe. For larger radii, on the other hand, the crystal is more jammed and due to the dragging along of surrounding small particles, a higher drag force is exerted on the probe.

Finally, we study quantitatively the reduction in drag force acting on the probe due to the surrounding particles being dragged along and advected around the probe. Data has been obtained for $1/\kappa = 20, 30$ and 50nm as well as drag velocities between 0.1 and $10\mu\text{m/s}$. In Fig. 4, force-velocity curves are compared for improved and conventional LD. For a clear presentation, data for $1/\kappa = 30\text{nm}$ and some intermediate values are omitted, but consistently fit into the presented range of results. It can be seen that the static friction effect is weaker if the hydrodynamic correction is not taken into account. This can be understood from Fig. 2: due to the hydrodynamic corrections, not only the probe but also a large number of close by crystal particles are moving. This leads to a much stronger rearrangement to be necessary in order to allow the particles to pass.

The experiments in [4] report a plateau of the force versus drag velocity curves for very small drag velocities $\leq 0.2\mu\text{m/s}$ and the authors suggest a finite yield stress as an explanation of this finding. Below a critical drag velocity, the inserted energy is mainly dissipated due to a local distortion of the colloidal crystal. In our simulations we are not able to reproduce this phenomenon within the limits of computationally feasible minimum drag velocities and statistical averaging. If a plateau would occur in

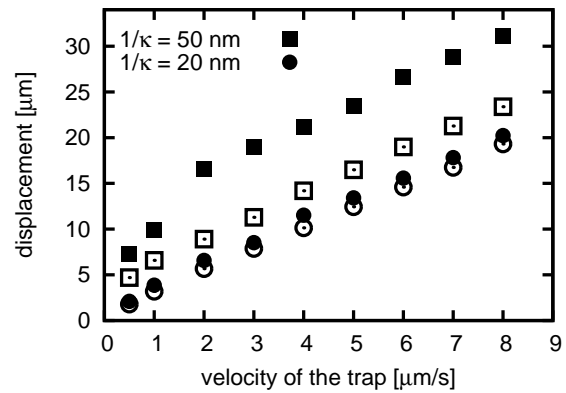


FIG. 4. Comparison of probe displacement in the trapping potential depending on the drag velocity from simulations with (full symbols) and without (open symbols) hydrodynamic correction and $1/\kappa = 20$ and 50nm . In all cases, the displacements for the simulations with hydrodynamic correction are higher than for the case with conventional LD. This is because, as can be seen from Fig. 2, due to the hydrodynamic corrections, not only the probe but also a large number of close by crystal particles are moving. Therefore, much more rearranging has to take place to allow them to pass.

our data for velocities below $0.5\mu\text{m/s}$, it would be hidden by the error bars of our measurements. However, our simulations do confirm the experimental finding of a power law behavior of the force versus drag velocity measurements. The exponents strongly depend on the inverse screening length $1/\kappa$. With hydrodynamic corrections we find 0.77 for $1/\kappa = 50\text{nm}$, 0.54 for $1/\kappa = 20\text{nm}$, where the latter is close to the value of 0.51 as reported in [4]. Without taking the flow field of the probe particle into account we obtain 0.86 and 0.62 , respectively.

IV. CONCLUSION

We conclude that in drag experiments as discussed in this letter, the assumption of the system to be overdamped is not valid and hydrodynamic interactions must not be neglected. By applying a modified LD scheme which includes the influence of the flow field around the driven probe, we demonstrated that the dynamics of the probe and the surrounding crystal are strongly influenced by the hydrodynamic interactions: the crystal particles around the probe are dragged along by its slip stream and advected around it. This significantly reduces the size of the depletion zone behind the probe. The drag force acting on the probe is increased or decreased depending on the density of the crystal.

Although the flow field generated by the moving probe is the most important hydrodynamic effect, efforts should be undertaken to perform simulations with full hydrodynamics using for example a combined method utilizing MD for the particles and a mesoscopic solver for the hy-

drodynamics [15–17]. This is, however, not easy, because the time step in the molecular dynamics simulation has to be small to properly model the steep Yukawa potentials. Therefore, the flow field would either have to be updated very often – which requires huge computational resources, or the simulation would have to use different time steps for MD and hydrodynamics – which might introduce unwanted artefacts. Furthermore, in particular for very low drag velocities, thermal fluctuations cause the necessity of averaging over very long simulation times in order to obtain reliable data. Another obstacle is the very different sizes of large and small particles which would force one to use a very small lattice spacing, if the

small particles are still to be resolved.

ACKNOWLEDGMENTS

We thank M. Rauscher, R. Dullens, and C. Bechinger for fruitful discussions and FOM (IPP IPoGII) and NWO/STW (VIDI grant 10787 of JH) for financial support. Computations were performed at the Jülich Supercomputing Centre and the Scientific Supercomputing Centre Karlsruhe.

-
- [1] V. Prasad, D. Semwogerere, and E. R. Weeks. *J. Phys. Condens. Matter*, 19:113102, 2007.
 - [2] R. Kesavamoorthy and C. B. Rao. *Bulletin of Materials Science*, 20:565, 1997.
 - [3] C. Reichhardt and C. J. Olson Reichhardt. *Phys. Rev. Lett.*, 92:108301, 2004.
 - [4] R. P. A. Dullens and C. Bechinger. *Phys. Rev. Lett.*, 107:138301, 2011.
 - [5] A. Pertsinidis and X. S. Ling. *Phys. Rev. Lett.*, 87:098303, 2001.
 - [6] P. T. Korda and D. G. Grier. *J. Chem. Phys.*, 114:7570, 2001.
 - [7] A. K. Arora and B. V. R. Tata. *Adv. in Col. Int. Sci.*, 78:49, 1998.
 - [8] G. Petekidis, D. Vlassopoulos, and P. N. Pusey. *J. Phys. Condens. Matter*, 16:S3955, 2004.
 - [9] A. Ashkin, J. M. Dziedzic, J. E. Bjorkholm, and S. Chu. *Opt. Lett.*, 11:288, 1986.
 - [10] D. O. Riese, G. H. Wegdam, W. L. Vos, R. Sprik, D. Fenistein, J. H. H. Bongaerts, and G. Grübel. *Phys. Rev. Lett.*, 85:5460, 2000.
 - [11] M. Rauscher, M. Krüger, A. Dominguez, and F. Penna. *J. Chem. Phys.*, 127:244906, 2007.
 - [12] C. Gutsche, F. Kremer, M. Krüger, M. Rauscher, J. Harting, and R. Weeber. *J. Chem. Phys.*, 129:084902, 2008.
 - [13] C. Gutsche, M. M. Elmahdy, K. Kegler, I. Semenov, T. Stangner, O. Otto, O. Ueberschär, U. F. Keyser, M. Krüger, M. Rauscher, R. Weeber, J. Harting, Y. W. Kim, V. Lobaskin, R. R. Netz, K. Kremer. *J. Phys. Condens. Matter*, 23:184114, 2011.
 - [14] L. D. Landau and E. M. Lifshitz. *Fluid mechanics*. Pergamon Press, 1959.
 - [15] M. Hecht, J. Harting, T. Ihle, and H. J. Herrmann. *Phys. Rev. E*, 72:011408, 2005.
 - [16] F. Jansen and J. Harting. *Phys. Rev. E*, 83:046707, 2011.
 - [17] A. J. C. Ladd and R. Verberg. *J. Stat. Phys.*, 104:1191, 2001.